European Radiology (2019) 29:5832–5843
https://doi.org/10.1007/s00330-019-06087-x

MAGNETIC RESONANCE

Assessment of the extracellular volume fraction for the grading of clear cell renal cell carcinoma: first results and histopathological findings

Lisa C. Adams[1] · Philipp Jurmeister[2] · Bernhard Ralla[3] · Keno K. Bressem[4] · Ute L. Fahlenkamp[1] · Guenther Engel[1] · Stefan Siepmann[1] · Moritz Wagner[1] · Bernd Hamm[1] · Jonas Busch[3] · Marcus R. Makowski[1]

Received: 29 August 2018 / Revised: 23 January 2019 / Accepted: 8 February 2019 / Published online: 18 March 2019

Abstract

Objectives To assess the potential of T1 mapping–based extracellular volume fraction (ECV) for the identification of higher grade clear cell renal cell carcinoma (cRCC), based on histopathology as the reference standard.

Methods For this single-center, institutional review board–approved prospective study, 27 patients (17 men, median age 62 ± 12.4 years) with pathologic diagnosis of cRCC (nucleolar International Society of Urological Pathology (ISUP) grading) received abdominal MRI scans at 1.5 T using a modified Look-Locker inversion recovery (MOLLI) sequence between January 2017 and June 2018. Quantitative T1 values were measured at different time points (pre- and postcontrast agent administration) and quantification of the ECV was performed on MRI and histological sections (H&E staining).

Results Reduction in T1 value after contrast agent administration and MR-derived ECV were reliable predictors for differentiating higher from lower grade cRCC. Postcontrast $T1_{diff}$ values ($T1_{diff}$ = T1 difference between the native and nephrogenic phase) and MR-derived ECV were significantly higher for higher grade cRCC (ISUP grades 3–4) compared with lower grade cRCC (ISUP grades 1–2) ($p < 0.001$). A cutoff value of 700 ms could distinguish higher grade from lower grade tumors with 100% (95% CI 0.69–1.00) sensitivity and 82% (95% CI 0.57–0.96) specificity. There was a positive and strong correlation between MR-derived ECV and histological ECV ($p < 0.01$, $r = 0.88$). Interobserver agreement for quantitative longitudinal relaxation times in the T1 maps was excellent.

Conclusions T1 mapping with ECV measurement could represent a novel in vivo biomarker for the classification of cRCC regarding their nucleolar grade, providing incremental diagnostic value as a quantitative MR marker.

Key Points

- *Reduction in MRI T1 relaxation times after contrast agent administration and MR-derived extracellular volume fraction are useful parameters for grading of clear cell renal cell carcinoma (cRCC).*
- *T1 differences between the native and the nephrogenic phase are higher for higher grade cRCC compared with lower grade cRCC and MRI-derived extracellular volume fraction (ECV) and histological ECV show a strong correlation.*
- *T1 mapping with ECV measurement may be helpful for the noninvasive assessment of cRCC pathology, being a safe and feasible method, and it has potential to optimize individualized treatment options, e.g., in the decision of active surveillance.*

Electronic supplementary material The online version of this article (https://doi.org/10.1007/s00330-019-06087-x) contains supplementary material, which is available to authorized users.

✉ Lisa C. Adams
Lisa.adams@charite.de

[1] Department of Radiology, Charité, Charitéplatz 1, 10117 Berlin, Germany

[2] Department of Pathology, Charité, Charitéplatz 1, 10117 Berlin, Germany

[3] Department of Urology, Charité, Charitéplatz 1, 10117 Berlin, Germany

[4] Department of Radiology, Charité, Hindenburgdamm 30, 12203 Berlin, Germany

Keywords Magnetic resonance imaging · Renal cell carcinoma · Neoplasm grading · Extracellular space · Extracellular matrix

Abbreviations

ADC	Apparent diffusion coefficient
AUA	American Urological Association
cRCC	Clear cell renal cell carcinoma
DWI	Diffusion-weighted imaging
ECM	Extracellular matrix
ECV	Extracellular volume fraction
ESM	Electronic supplementary material
H&E	Hematoxylin and eosin
ICC	Intraclass coefficient
ISUP	International Society of Urological Pathology
MOLLI	Modified Look-Locker inversion recovery
ROC	Receiver operating characteristic curve
ROI	Region of interest
SNR	Signal-to-noise ratio
TER	Tumor enhancement ratio

Introduction

Renal cell carcinoma (RCC) is a frequent malignancy, representing 2–3% of adult cancers [1]. Accounting for approximately 90% of all kidney malignancies, it comprises different RCC types with individual genetic and histopathologic characteristics [2]. Out of these types, clear cell renal cell carcinoma (cRCC) is the most common [3]. Apart from the tumor type, stage and grading are important prognostic factors for the prediction of cancer-specific survival. The International Society of Urological Pathologists (ISUP) stratified cRCC into a four-tier system, with lower grade tumors (ISUP 1–2) showing an excellent 10-year survival rate of approximately 95% compared with about 60% for higher grade RCC (ISUP 3–4) [4]. While percutaneous biopsies can increase chances of a preoperative pathologic diagnosis, they are associated with procedural complications, potential sampling errors, and inaccurate tumor grading or subtyping [5]. With a lot of renal masses being incidental diagnoses on routine clinical imaging, image-based tumor grading would be of clinical relevance [6, 7], as it could aid in triaging patients to the best individual therapy, e.g., focal therapy or active surveillance.

MR-based T1 mapping is a promising diagnostic tool for quantitative measurement and characterization of tissues, also allowing for a noninvasive quantification of the ECV [8].

Previous research demonstrated an increase of the ECV in different tumors with evidence that the extracellular matrix (ECM) represented a modulator of tumor growth, proliferation, or invasion [9]. Compounds of ECV glycoproteins have also been shown to contribute to the development and progression of cRCC [10, 11].

The aim of this study was to assess the potential of T1 mapping, with derived ECV before and after the application of contrast agents, for the identification of higher cRCC. Histopathology with ISUP grading served as the reference standard.

Methods

Study design and population

This prospective study was institutional review board–approved and written informed consent was obtained from all participants prior to the examination. Between January 2017 and August 2018, 37 consecutive patients with suspected cRCC, who agreed to participate and had no contraindications to MR or prior focal ablation, were referred to our department for abdominal MRI examinations with application of contrast agents (refer to Fig. 1 for an overview of the study workflow).

Imaging protocol

All examinations were performed on a 1.5-T MR scanner (Avanto; Siemens Medical Solutions) with a dedicated 16-channel body phased-array coil. The patients underwent a clinical routine image protocol of the kidneys and in addition received native and postcontrast steady-state precession single-shot modified Look-Locker inversion recovery (MOLLI) sequences in coronal planes, adjusted to the long axis of both kidneys. The routine image protocol of the kidneys included a coronal and sagittal T2 HASTE image, a native axial 3D T1 FLASH image, a T1 FLASH angiography, and a fat-saturated T1 3D VIBE sequence for the delayed or excretory phase imaging (refer to Table 1 for tabulated magnetic resonance imaging parameters). Gadoterate meglumine (Dotarem®) was used as contrast agent. Coronal 3D FLASH sequences were obtained dynamically in the corticomedullary and nephrogenic phases. With bolus tracking, the arterial phase could be accurately timed to peak enhancement of the abdominal aorta. The corticomedullary phase was acquired approximately 20 s after the start of the arterial phase and the nephrogenic phase was initiated another 70 s after the start of the corticomedullary phase. The calculation of the T1 maps was automated on a pixel-by-pixel basis, with the resulting pixel-by-pixel maps being displayed through a customized 12-bit lookup table with a visible color map immediately after the acquisition. In this map, the signal intensity of each of the pixels reflects their absolute T1 values.

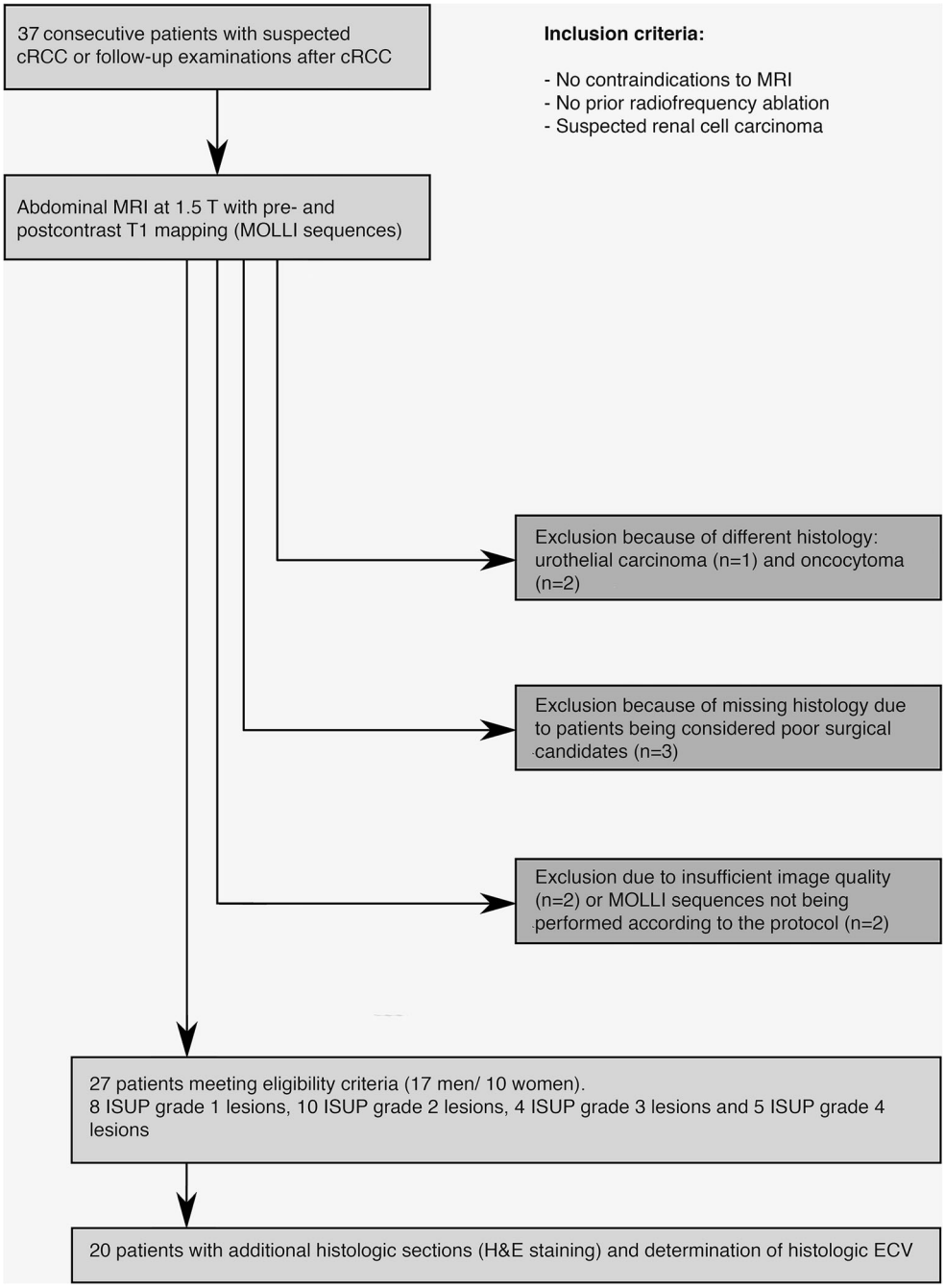

Fig. 1 Workflow of participants through the study. Diagram illustrating the flow of study participants and showing the reasons for exclusion as well as the final study population, which met the eligibility criteria

Phantom of estimated T1 values

To test the accuracy of estimated T1 values, a phantom with T1 values in the same range as those observed in cRCC patients was developed, based on a dilution series of gadolinium (gadoterate meglumine) from 1:2000–1:20,000 in steps of 500. The samples were filled in 50-ml Falcon tubes. For MR scanning, the tubes were placed in a plastic box, filled with water, and sorted in order of descending concentrations (refer to Fig. S1 and ESM Table S1).

Imaging analysis

All images were analyzed using Visage 7.1 (Visage Imaging). Assessment of T1 mapping (MOLLI) was performed by two independent radiologists, blinded to the clinical information and histologic grading, in two different reading sessions. For each patient, circular ROIs of maximum size were placed within the most homogeneous and hyperintense portion of solid tumor area on the basis of visual assessment in postcontrast sequences. Regions of necrosis, cystic degeneration, and hemorrhage were avoided and identified by lack of

Table 1 Tabulated MR imaging parameters

	Sequence			
	T1 FLASH	T2 HASTE	MOLLI	T1 3D FLASH
Scan plane	Axial	Coronal	Coronal	Coronal
Voxel size (mm)	1.4 × 1.1 × 4.0	1.7 × 1.3 × 5.0	1.9 × 1.3 × 4.0	1.6 × 1.0 × 1.4
Number of slices	60	25	1	1
TR/TE (ms)	186/4.76	800/89	912/1.16	2.88/0.98
Averages	1	1	2	1
FoV (mm)	340	400	400	500
Flip angle (°)	70	170	35	25
Matrix	320	320	320	512
Bandwidth (Hz/Px)	260	422	1042	440
Fat saturation	None	None	None	Yes
Parameter map type	–	–	T1 map	–
Number of inversions	–	–	3	–
MOLLI TI start (ms)	–	–	153	–
MOLLI T1 increment (ms)	–	–	80	–
MOLLI T1 trigger delay (ms)	–	–	160	–

MOLLI Modified Look-Locker inversion recovery, *FLASH* Fast low angle shot magnetic resonance imaging

enhancement. Apart from the ROI measurements within the solid parts of the cRCC, additional circular ROIs were placed in the renal cortex and medulla. The differences ($T1_{diff}$) between the native and the nephrogenic T1 values and the difference between the nephrogenic and the excretory phases were calculated ($T1_{ex}$), averaged over two observers:

$$T1_{diff} = 0.5 \times \begin{pmatrix} \text{native.tumor.T1 (observer1)} \\ + \text{native.tumor.T1 (observer2)} \end{pmatrix} - 0.5 \times \begin{pmatrix} \text{postcontrast.tumor.T1 (observer1)} \\ + \text{postcontrast.tumor.T1 (observer2)} \end{pmatrix}.$$

T1 values for pre- and postcontrast blood were determined by ROIs drawn in the center of the descending aorta. The ECV was calculated based on the individual hematocrit and the pre- and postcontrast T1 values of the cRCC and the blood pool according to the following formula [12]:

$$ECV = \begin{pmatrix} 1 - \text{haematocrit} \times \begin{pmatrix} (1/\text{T1cRCC.post}) \\ -(1/\text{T1cRCC.pre}) \end{pmatrix} \\ /((1/\text{T1blood.post}) - (1/\text{T1blood.pre})) \times 100\% \end{pmatrix}.$$

A blood sample was obtained prior to the scanning to control for the kidney parameters and for measurement of the hematocrit. To compare the results of T1 mapping with standard MR angiography, a relative tumor enhancement ratio (TER) [13] was calculated.

$$TER = \begin{pmatrix} (\text{Post} - \text{contrast.cRCC} - \text{enhancement}) \\ -(\text{Unenhanced.cRCC}) \end{pmatrix} / \begin{pmatrix} (\text{Post} - \text{contrast.renal cortex} - \text{enhancement}) \\ -(\text{Unenhanced.renal.cortex}) \end{pmatrix}.$$

Calculation of histological extracellular volume fraction

The histological specimens taken from the cRCC were fixed in formalin, embedded in paraffin wax, sectioned at 2 μm, and stained with hematoxylin and eosin (H&E) for estimation of the ECV. Two representative magnification (× 50) tiled digital images, one from a central and the other from a periphery region, were acquired per patient (Zeiss-LSM-710, Carl Zeiss). In the next step, a quantitative analysis was performed with ImageJ (ImageJ-1.50i, Wayne Rasband, National Institutes of Health). The H&E-colored images analyzed with automatic thresholding to achieve the best possible separation of intracellular from ECV. ECV was calculated as the percentage of the selected ECV area, divided by the total depicted cRCC area.

ISUP grading

cRCC was examined by a pathologist, who was blinded to the clinical information and the MOLLI assessment (index test results), and classified into four ISUP grades [13]. ISUP grading is based on the evaluation of nucleolar prominence, with

grade 4 tumors showing a high degree of polymorphism and rhomboid and/or sarcomatoid morphology [13].

Statistical analysis

Continuous variables were expressed as means ± standard deviations, if applicable. Student's *t* tests were used for continuous variables and the Mann-Whitney *U* test was used for intergroup differences. Boxplots were employed to display the distribution of the averaged T1 values along the different groups. To estimate the optimal cutoff T1 value for the identification of higher grade cRCC, a receiver operating characteristic curve (ROC) analysis was performed, prioritizing sensitivity over specificity for the exploratory selection of the optimal cutoff value. Interobserver agreement was calculated with the intraclass correlation coefficient (ICC) and visualized by Bland-Altman plots. *P* values < 0.05 were considered statistically significant. All statistical analysis was performed with "R" Statistical Software (Version 3.2.2, R Development Core Team, 2015).

Results

Quantitative measurements, quantitative analysis, and interobserver agreement

A total of 27 patients were included in the present study (62 ± 12.4 years). An overview of the study characteristics is given in Table 2. The histological grading of the patients revealed 8 ISUP grade 1 lesions, 10 ISUP grade 2 lesions, 4 ISUP grade 3 lesions, and 5 ISUP grade 4 lesions. Mean maximum cRCC diameter was 6.35 ± 4.22 cm and mean ROI sizes were 10.7 cm^2 ± 9.8 cm^2. There was no significant difference in men and women regarding tumor size or between age and ISUP grade ($p > 0.05$). For 20 of the patients, additional histologic sections for H&E staining were available. The time interval between MRI imaging and surgical excision was 27.7 ± 21.4 days.

Identification of higher grade cRCC

Native and postcontrast T1 relaxation times were measured and averaged over two observers. The higher the ISUP grade, the higher the difference between the native and nephrogenic phase, enabling a reliable distinction between different ISUP grades (see Fig. 2 and Electronic Supplementary Material (ESM) Fig. S2). MR-derived ECV also allowed a convincing differentiation between each ISUP grade ($p < 0.001$).

$T1_{nephrogenic}$, $T1_{excretory}$ and $T1_{diff}$, $T1_{ex}$, and MR-derived ECV were calculated, whereby $T1_{diff}$ and MR-derived ECV were the best predictors for the different cRCC grades (see Fig. 3 and Fig. S3). Multivariate analysis demonstrated a statistically significant difference in $T1_{diff}$ values between lower grade (ISUP 1, 2) and higher grade (ISUP 3, 4) ($p < 0.001$) cRCCs, but also between ISUP grades 1–2 and ($p < 0.01$), ISUP grades 2–3 ($p < 0.001$), and ISUP grades 3–4 ($p < 0.05$). This equally applied to MR-derived ECV.

Average $T1_{diff}$ values were 414.8 ms ± 151.2 ms for ISUP grade 1, 668.5 ms ± 127.0 ms for ISUP grade 2, 829.5 ms ± 42.0 ms for ISUP grade 3, and 966 ms ± 34.6 ms for ISUP grade 4. Higher grade cRCC (ISUP grades 3, 4) showed significantly longer $T1_{diff}$ values compared with lower grade tumors (ISUP grades 1, 2), indicating a higher gadolinium

Table 2 Characteristics of the study population

Number of patients with cRCC (men/women)	27 (17/10)
Median age of patients with cRCC (SD)	62 (12.4)
Partial nephrectomy (%)	48.1% ($n = 13$)
Radical nephrectomy (%)	44.4% ($n = 12$)
Biopsy (%)	7.4% ($n = 2$)
Average nephrogenic T1 values (SD) for the renal parenchyma	
Renal cortex	1026.8 ms (65.6 ms)
Renal medulla	1254.8 ms (81.9 ms)
Average $T1_{diff}$ values for cRCC (SD, number, %)	
ISUP grade 1	414.8 ms (151.2 ms, 8, 29.6)
ISUP grade 2	668.5 ms (127.0 ms, 10, 37.0)
ISUP grade 3	829.5 ms (42.0 ms, 4, 14.8)
ISUP grade 4	966 ms (34.6 ms, 5, 18.6)
Average $T1_{nephrogenic}$ values for cRCC (SD)	
ISUP grade 1	491.6 ms (60.9 ms)
ISUP grade 2	408.8 ms (26.2 ms)
ISUP grade 3	373.9 ms (51.1 ms)
ISUP grade 4	383.3 ms (60.7 ms)

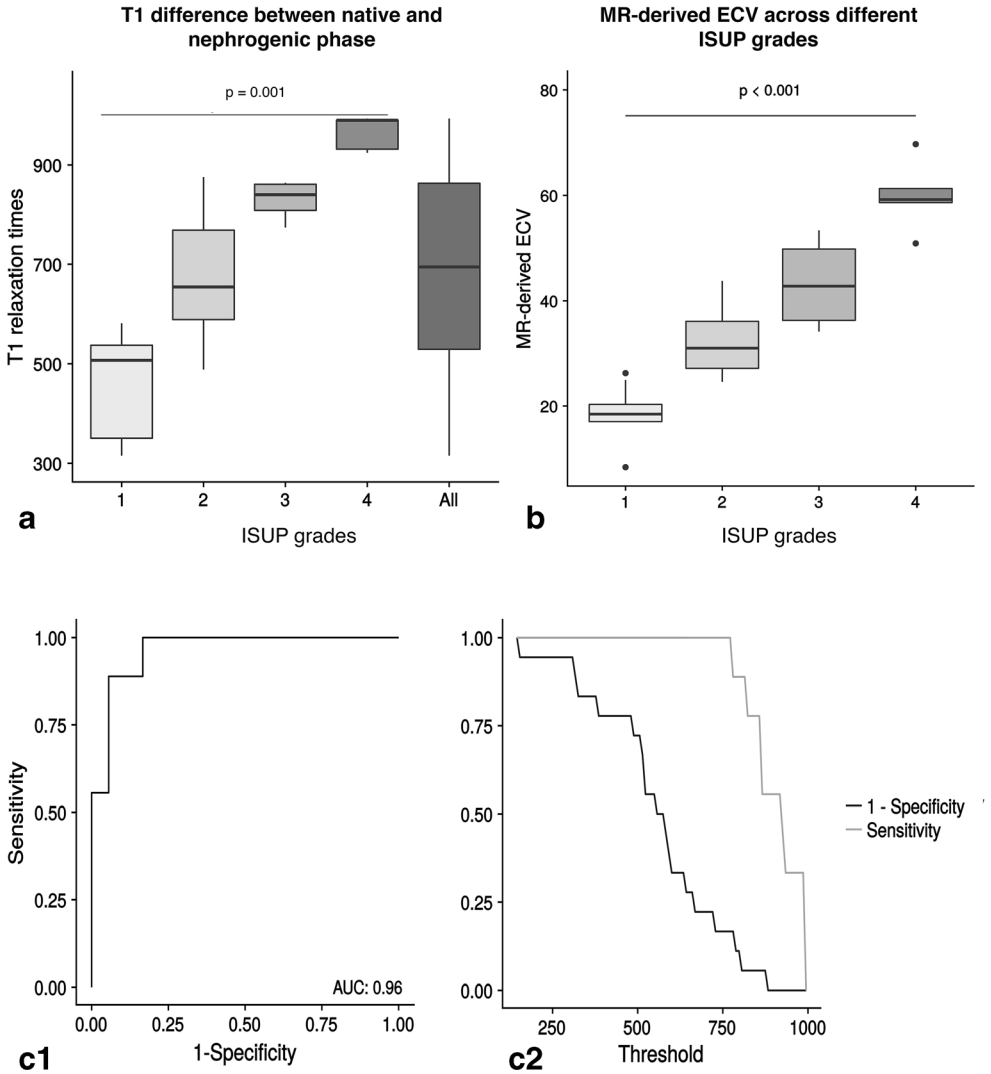

Fig. 2 Distribution of differences in T1 ($T1_{diff}$) and in the extracellular volume fraction across different ISUP grades. The upper left part of the figure (a) displays the T1 differences between native and nephrogenic phases across different ISUP grades using boxplots. T1 differences between the native and the nephrogenic phase are higher for higher grade cRCC (ISUP grades 1 and 2) compared with lower grade cRCC (ISUP grades 3 and 4). The bottom and top of the boxes represent the first and third quartiles, the band in the box represents the median, and the ends of the whiskers indicate the minimum and maximum. The upper right part of the figure (b) shows the MR-derived extracellular volume fraction (ECV) in % values across different ISUP grades with boxplots. Higher grade cRCC shows higher ECV values compared with lower grade cRCC. The lower left part of figure (c1) illustrates the diagnostic performance of T1 mapping as a binary classifier in discriminating between ISUP grades 1 and 2 and 3 and 4. In this context, the T1 threshold is varied using a receiver operating characteristic curve (ROC curve). The corresponding area under the curve (AUC) is 0.96. The lower right part of the figure (c2) displays the respective sensitivity and specificity values plotted against their corresponding threshold

uptake. ROC curve analysis showed a cutoff value of 700 ms (for $T1_{diff}$) to detect higher grade cRCC with a sensitivity of 100% (95% CI 0.69–1.00) and a specificity of 82% (95% CI 0.57–0.96) (refer to Table 3 for confusion matrix and to Fig. 3 for case examples).

Association of MR-derived ECV and histological ECV

The mean histological ECV across different cRCC grades was 35.9% ± 15.9%, while the mean MR-derived ECV was 30.6% ± 11.2% (Fig. 4). Patients with higher grade cRCC showed significantly higher MR-derived and histological ECV. Spearman's correlation analysis revealed strong correlation between MR-derived ECV and histological ECV ($p < 0.01$, $r = 0.88$) (Fig. 5). $T1_{diff}$ values also strongly correlated with the histological ECV ($r = 0.81$).

Imaging of higher grade cRCC based on standard MR angiography

The tumor-to-cortex enhancement ratios ($TER_{corticomedullary}$ and $TER_{nephrogenic}$) showed no significant difference between

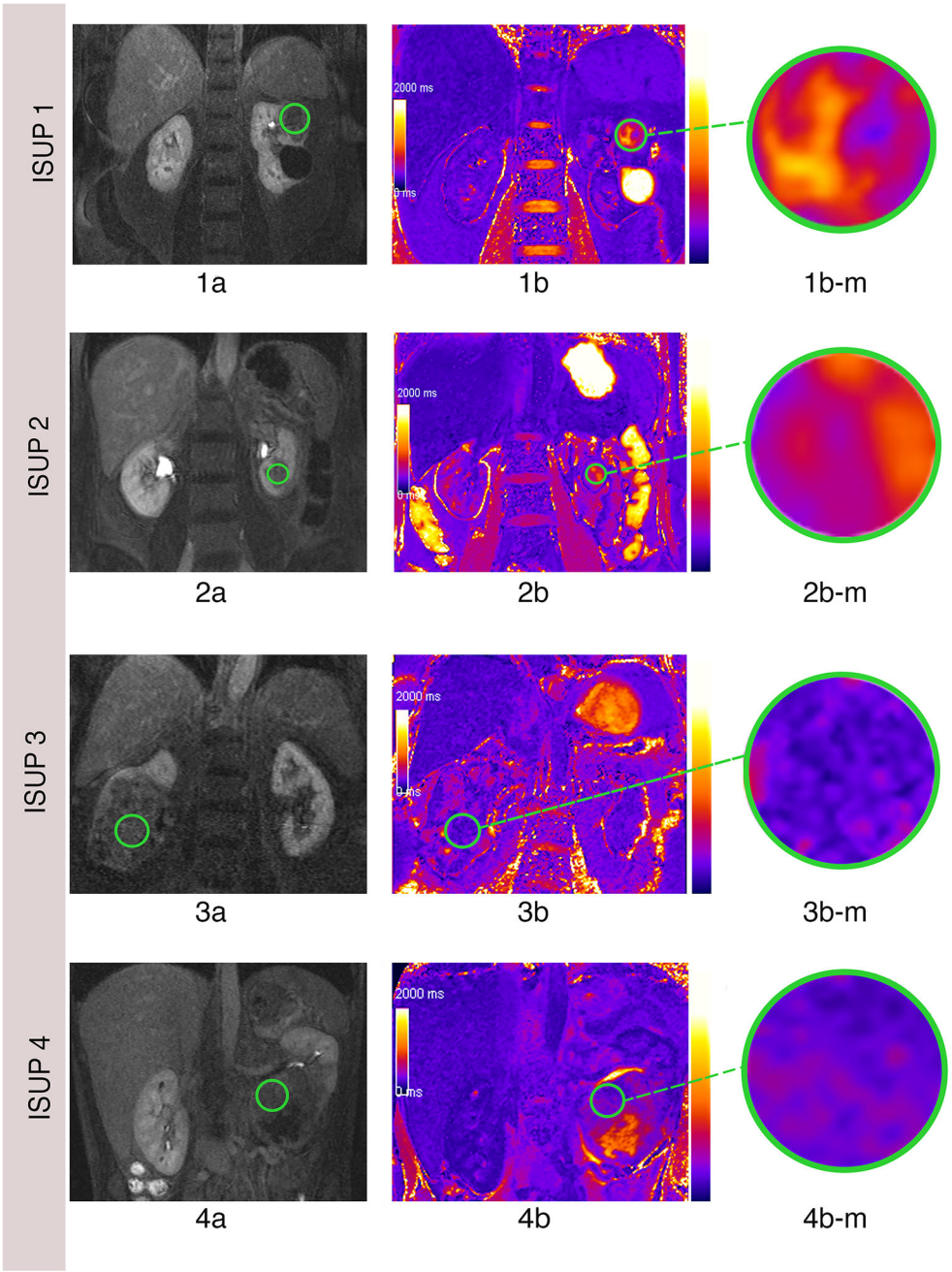

Fig. 3 Postcontrast T1 mapping images of lower and higher grade cRCC. (1a) Postcontrast T1 FLASH image with exemplary ROI placement in a homogenously bright appearing area (refer to "Methods" section for more details). (1b) Corresponding MOLLI image, showing a relatively high T1 relaxation time. (2a) Postcontrast T1 FLASH image of a 63-year-old woman with a low-grade (ISUP 2) cRCC of the right kidney and exemplary ROI placement in a solid tumor area. (2b) Corresponding postcontrast MOLLI image, showing an intermediately high T1 signal. (3a) Postcontrast T1 FLASH image of a 76-year-old woman with a higher grade (ISUP 3) cRCC of the right kidney and exemplary ROI placement. (3b) Corresponding postcontrast MOLLI image, showing a relatively low T1 signal. (4a) Postcontrast T1 FLASH image of a 47-year-old man with a high-grade (ISUP 4) cRCC of the left kidney with a central necrotic area and exemplary ROI placement in a solid tumor area. (4b) Corresponding postcontrast MOLLI image, again showing a relatively low T1 signal. The high T1 signal in the center with lack of enhancement in the conventional MR angiography corresponds to a necrotic area and was excluded from ROI placement. (1b-m, 2b-m, 3b-m, and 4b-m) Corresponding magnifications of the ROIs placed in (1b), (2b), (3b), and (4b)

Table 3 Confusion matrix for the calculation of sensitivity and specificity

MR native T1 mapping (index test)	Histology (reference standard)		Total
	Confirmed higher grade cRCC	Confirmed lower grade cRCC	
Higher grade cRCC (ISUP grades 3 and 4)	10	3	13
Lower grade cRCC (ISUP grades 1 and 2)	0	14	14
Total	10	17	27

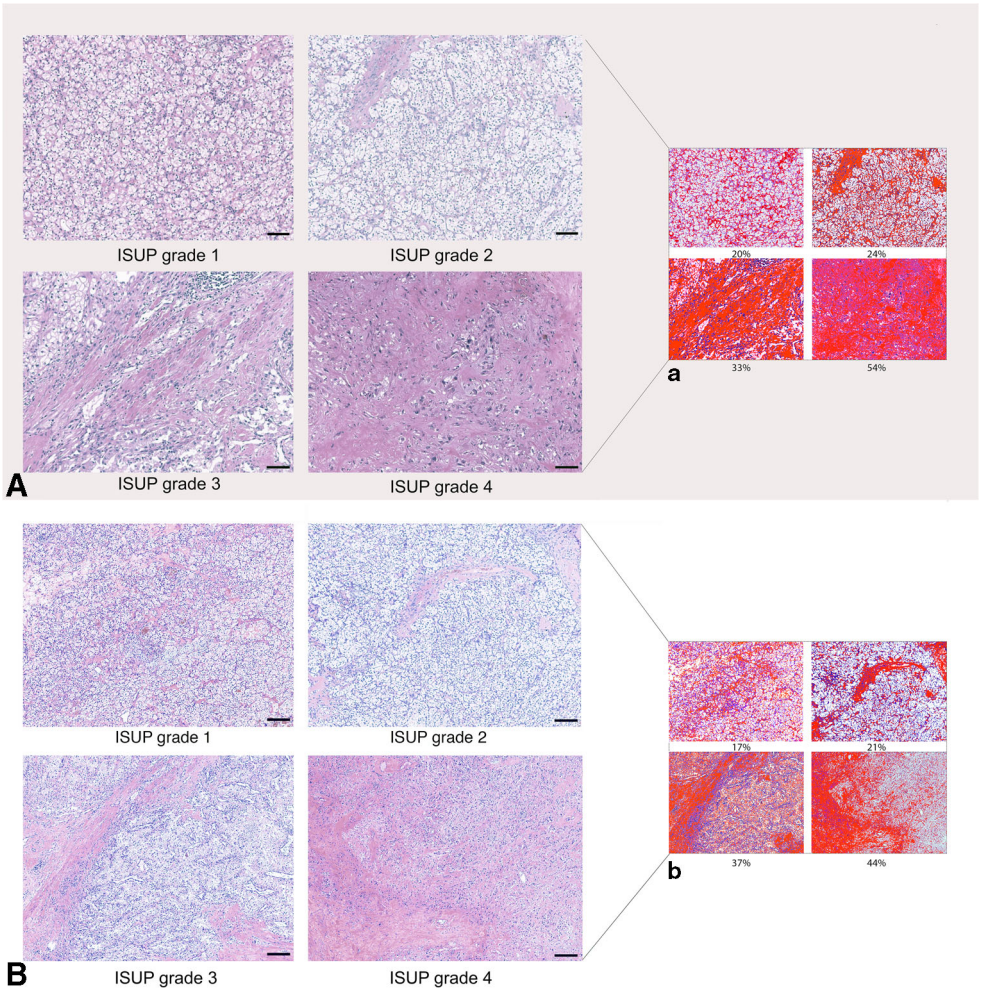

Fig. 4 Measurement of the extracellular volume fraction. Examples of magnified (× 50) images in hematoxylin and eosin–stained sections (**A**) with a bar indicating 200 μm and (after digital magnification) (**B**) with a bar indicating 100 μm. Magnification images with × 50 were used for automated analysis with ImageJ to assess the extracellular volume fraction (**a** and **b**). (**a**) and (**b**) Extracellular area selection in ImageJ after color thresholding. Examples demonstrated in this figure correspond to 20%, 24%, 33%, and 54% of extracellular volume fraction for ISUP grades 1 to 4 for a periphery region (with an exemplary higher digital magnification for better visualization) and to 17%, 21%, 37%, and 44% for a central region of the tumor

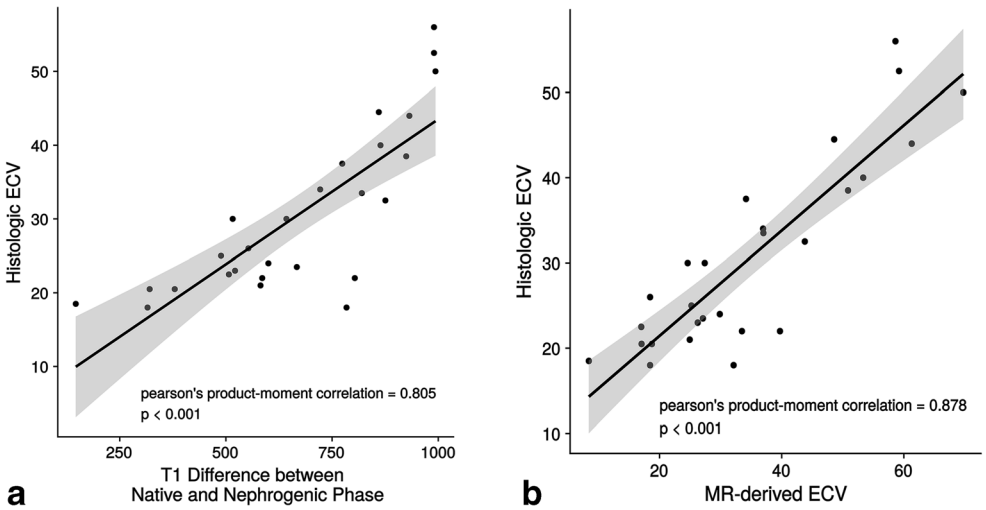

Fig. 5 Association between T1 differences and MR-derived extracellular volume fraction (ECV) and histological ECV. Sections were stained with hematoxylin and eosin and the extracellular volume fraction was calculated as the percentage of the extracellular space, divided by the total depicted cRCC area. **a** T1 differences between the native and nephrogenic phase values showed a very strong correlation with the histological extracellular volume fraction (correlation coefficient $r = 0.80$), with the gray-colored area indicating confidence intervals. **b** MRI-derived ECV also showed a very strong correlation with the histological extracellular volume fraction (correlation coefficient $r = 0.88$), again with the gray-colored area indicating confidence intervals

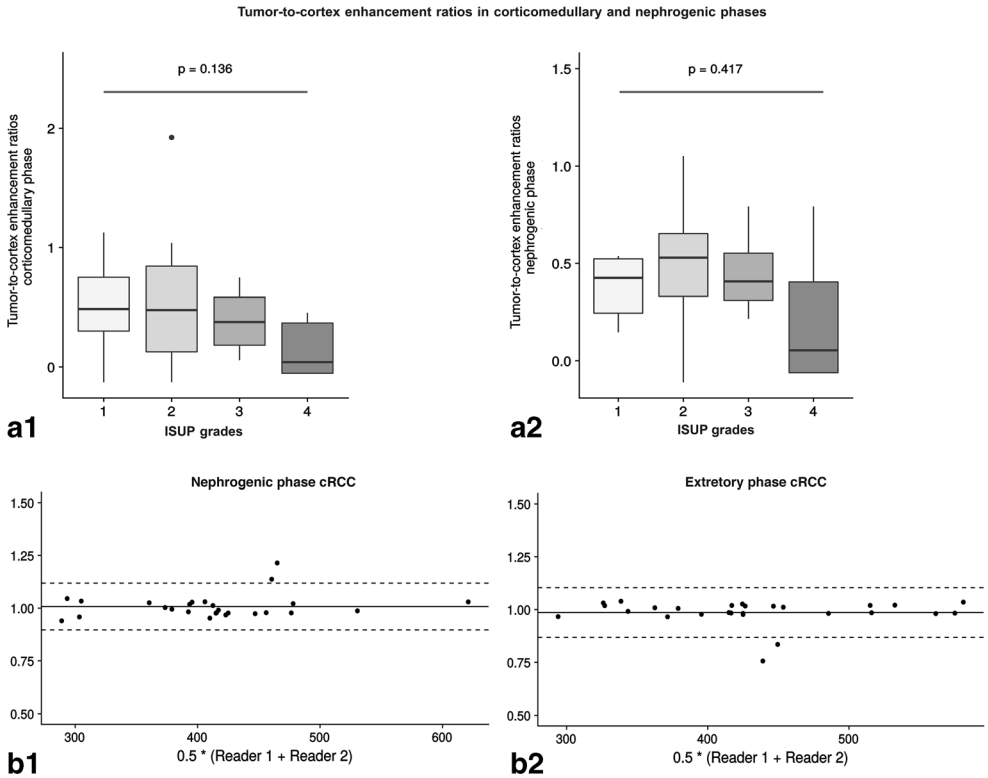

Fig. 6 Tumor-to-cortex enhancement ratios for the corticomedullary and nephrogenic phases and interobserver agreement of postcontrast T1 values of cRCC in the nephrogenic and excretory phase. (a1) Tumor-to-cortex enhancement ratios across different ISUP grades in the corticomedullary phase with a trend towards lower tumor-to-cortex enhancement ratios in higher grade tumors, which, however, does not reach statistical significance ($p = 0.136$). (a2) Comparably lower tumor-to-cortex enhancement ratios across different ISUP grades in the nephrogenic phase with no significant difference in tumor-to-cortex enhancement ratios between the different ISUP grades ($p = 0.417$). Bland-Altman plots illustrate the interobserver variability for postcontrast cRCC T1 values in the nephrogenic (b1) and excretory (b2) phases. Specifically, the mean ratios were 1.01 (CI 0.9–1.12) for the cRCC T1 times in the nephrogenic phase and 0.99 (CI 0.87–1.1) for the excretory phase. The mean ratio of the data is illustrated by the central horizontal line. The upper and lower reference lines indicate the upper and lower limits of agreement (96% confidence intervals)

high- and low-grade cRCCs (corticomedullary and medullary: $p > 0.05$) (for visual illustration, refer to Fig. 6).

Agreement of interobserver measurements

Postcontrast quantitative T1 values for both the nephrogenic and the excretory phases demonstrated a high interobserver agreement. Mean ratios were 1.01 (95% CI 0.9–1.12) for the cRCC T1 times in the nephrogenic phase and 0.99 (95% CI 0.87–1.1) for the excretory phase (refer to Fig. 6). There was also an excellent interobserver agreement for the cRCC nephrogenic T1 values (ICC 0.94, 95% CI 0.89–0.98) and the T1 values in the excretory phase (ICC 0.86, 95% CI 0.73–0.91).

Discussion

This prospective study suggests that T1 mapping may enable a noninvasive differentiation of higher grade from lower grade renal cell carcinoma, based on postcontrast changes in longitudinal relaxation times. Higher grade cRCC showed significantly higher $T1_{diff}$ values and higher percentages of MR-derived ECV, which, furthermore, correlated well with the histological ECV.

Patients with a high-grade cRCC were shown to have a significantly higher risk for cancer-specific death compared with lower grade cRCC patients [14]. Image-based tumor grading would offer the chance to improve prognosis assessment and prior patient information as well as preoperative planning. Due to elderly and comorbid patients with small renal masses having a low RCC-specific mortality versus a significant competing cause mortality, active surveillance is increasingly recommended in selected cases [15, 16]. However, at present, there are neither objective criteria for the selection of adequate patients nor a uniform definition for active surveillance. To this end, image-based tumor grading could facilitate the appropriate selection of patients suitable for active surveillance. Furthermore, it could also aid in identifying patients suitable for other less invasive forms of therapy, such as focal therapy, which may help to prevent cases of upstaging after partial nephrectomy and to identify

patients eligible for immunotherapy [17]. In addition, an increased use of renal mass biopsies for the diagnosis and risk stratification of patients with renal masses suspicious of renal cancer, which was recently recommended by the 2017 American Urological Association (AUA) Renal Mass and Localized Renal Cancer Guidelines, could be reduced in favor of a noninvasive image-based approach [15]. Generally, image-based grading with T1 mapping would be particularly helpful as well as potentially cost-effective in patients with smaller renal masses and comorbidities/higher risk of perioperative complications [18]. Finally, the T1 mapping approach chosen in the present study would be relatively easy to implement in clinical practice due to already being commercially available.

Chemical shift imaging and diffusion-weighted imaging (DWI) are other quantitative MR techniques used to characterize biological tissues. In chemical shift imaging, a decrease in signal intensity on opposed-phase gradient-echo images displays the ratio of lipid content to total tissue amount in each voxel [17]. Chemical shift imaging was previously shown to be potentially helpful for the visualization of intracellular lipid and glycogen in cRCC [18]. More recently, Karlo et al found a decrease in signal intensity of more than one-quarter to be diagnostic for cRCC, while they found no difference in signal intensity for the different cRCC grades [17].

DWI, other than T1 mapping and chemical shift imaging, relies on the measurement of the random motion of water molecules within tissues to use in qualitative/quantitative evaluations based on the apparent diffusion coefficient (ADC), with highly cellular tissues generally showing lower diffusion coefficients [19]. The ADC was previously shown to be a potential noninvasive quantitative biomarker for tumor characterization [20]. With regard to RCC, there is a wide range of reported ADC values, possibly reflecting the dependence on MR scanners/sequence parameters [21]. Generally, RCC tumor tissue was shown to display lower ADC values compared with benign tissue, with some research reporting different ADC values for cRCC and other renal tumors [22–24]. A systematic review by Kang et al suggested a moderate accuracy of DWI for the prediction of renal malignancy and high-grade cRCC, while the performance of DWI to ascertain clear cell histologic grade was considered unclear [25]. Similarly, a more recent meta-analysis by Woo et al also reported a moderate diagnostic performance of DWI for differentiation of high- from low-grade cRCC [26]. So far, there is limited research on the comparison of DWI and T1 mapping, adding to the importance of future studies in this area [27, 28].

Recent studies showed an association between an abundance of extracellular matrix proteins and ECV/T1 values [29, 30]. Furthermore, it was found that metastases, tumor progression, or poor prognosis in cRCC was related to the upregulation of extracellular matrix genes and proteins, especially in higher grade cRCC [10, 31–33]. By contrast, histologically, well-differentiated cRCCs are composed of relatively large tumor cells with clear cytoplasm and narrow intercellular spaces, which might in part explain the relatively low T1 values and ECV in lower grade cRCC [34]. As necrosis does occur not only in the form of macroscopically visible areas of necrosis but also in the form of microscopic necrosis, inclusion of some microscopic necrosis areas cannot be excluded, potentially affecting $T1_{diff}$ and making the differentiation from higher grade cRCC more difficult. In lower grade cRCC, presence of microscopic cystic degeneration may result in an increase of $T1_{diff}$, potentially leading to an upgrading of lower grade tumors. In our study, we showed differences in quantitative T1 values for the four cRCC grades, with $T1_{diff}$ being highest for ISUP grade 4 tumors and lowest for ISUP grade 1 cRCC, indicating a higher gadolinium uptake in higher grade cRCC. Even though based on $T1_{diff}$ and MR-derived ECV, it was possible to distinguish all four grades of cRCC with statistical significance, a two-tier differentiation was chosen due to the small number of patients, especially regarding higher grade cRCC. However, a four-tier sub-differentiation appears to be very promising in our proof-of-concept study.

The present study has several limitations. First, being a proof-of-concept study, it is based on a single-center design and includes only a small number of patients. Another limitation is that scan-rescan variation was not tested and that only one scanner from one vendor was used; because of this, the results may not be generalizable to all institutions. Due to a "bolus-only" approach in the present study, ECV values over 40% might have been overestimated compared with slow infusion techniques [35]. Besides, there is an overlap between the fourth quartile of ISUP 2 and the first to fourth quartile of ISUP 3 (refer to Fig. 2), indicating that up to one-quarter of tumors with ISUP grade 2 might be over graded based on T1 mapping, using the proposed cutoff for $T1_{diff}$ values. While postcontrast T1 mapping is not a perfect test, which is also shown by its specificity of 82%, it still allows to detect higher grade tumors (ISUP 3, 4) with 100% sensitivity. Furthermore, even though this study validated the different cRCC grades against the ECV in cRCC samples, the tissue samples only represented relatively small tumor sections, which cannot be accurately located based on MRI; because of this, a sampling bias cannot be excluded. Also, this study only examined cRCC instead of a wider range of RCC subtypes. Finally, another practical limitation of T1 mapping is that especially for younger patients with lower risk of surgical complications, the potential clinical impact of a preoperative tumor grading may be limited, since curative surgery remains the primary approach.

In conclusion, quantitative T1 mapping with image-based ECV measurement could represent a novel in vivo biomarker for the differentiation of lower and higher grade cRCCs, reflecting intrinsic tissue properties and contrast agent uptake

in the extracellular space. As a consequence, in vivo characterization of cRCC with T1 mapping could potentially optimize individualized treatment options, assisting in the selection of less invasive therapeutic options.

Acknowledgements LCA and BR are grateful for their participation in the BIH Charité - Junior Clinician Scientist Program funded by the Charité - Universitaetsmedizin Berlin and the Berlin Institute of Health. JB is participant in the BIH – Twinning Grant Program funded by the Charité - Universitaetsmedizin Berlin and the Berlin Institute of Health. MRM is funded by the Deutsche Forschungsgemeinschaft (DFG, German Research Foundation) – SFB 1340/1 2018, 5943/31/41.

Funding The authors state that this work has not received any funding.

Compliance with ethical standards

Guarantor The scientific guarantor of this publication is Lisa C. Adams.

Conflict of interest The authors of this manuscript declare relationships with the following companies: Bernd Hamm has received research grants for the Department of Radiology, Charité – Universitätsmedizin Berlin from the following companies: 1. Abbott, 2. Actelion Pharmaceuticals, 3. Bayer Schering Pharma, 4. Bayer Vital, 5. BRACCO Group, 6. Bristol-Myers Squibb, 7. Charite research organisation GmbH, 8. Deutsche Krebshilfe, 9. Dt. Stiftung für Herzforschung, 10. Essex Pharma, 11. EU Programmes, 12. Fibrex Medical Inc., 13. Focused Ultrasound Surgery Foundation, 14. Fraunhofer Gesellschaft, 15. Guerbet, 16. INC Research, 17. lnSightec Ud., 18. IPSEN Pharma, 19. Kendlel MorphoSys AG, 20. Lilly GmbH, 21. Lundbeck GmbH, 22. MeVis Medical Solutions AG, 23. Nexus Oncology, 24. Novartis, 25. Parexel Clinical Research Organisation Service, 26. Perceptive, 27. Pfizer GmbH, 28. Philipps, 29. Sanofis-Aventis S.A, 30. Siemens, 31. Spectranetics GmbH, 32. Terumo Medical Corporation, 33. TNS Healthcare GMbH, 34. Toshiba, 35. UCB Pharma, 36. Wyeth Pharma, 37. Zukunftsfond Berlin (TSB), 38. Amgen, 39. AO Foundation, 40. BARD, 41. BBraun, 42. Boehring Ingelheimer, 43. Brainsgate, 44. PPD (Clinical Research Organisation), 45. CELLACT Pharma, 46. Celgene, 47. CeloNova BioSciences, 48. Covance, 49. DC Deviees, Ine. USA, 50. Ganymed, 51. Gilead Sciences, 52. Glaxo Smith Kline, 53. ICON (Clinical Research Organisation), 54. Jansen, 55. LUX Bioseienees, 56. MedPass, 57. Merek, 58. Mologen, 59. Nuvisan, 60. Pluristem, 61. Quintiles, 62. Roehe, 63. Sehumaeher GmbH (Sponsoring eines Workshops), 64. Seattle Geneties, 65. Symphogen, 66. TauRx Therapeuties Ud., 67. Accovion, 68. AIO: Arbeitsgemeinschaft Internistische Onkologie, 69. ASR Advanced sleep research, 70. Astellas, 71. Theradex, 72. Galena Biopharma, 73. Chiltern, 74. PRAint, 75. lnspiremd, 76. Medronic, 77. Respicardia, 78. Silena Therapeutics, 79. Spectrum Pharmaceuticals, 80. St. Jude., 81. TEVA, 82. Theorem, 83. Abbvie, 84. Aesculap, 85. Biotronik, 86. Inventivhealth, 87. ISA Therapeutics, 88. LYSARC, 89. MSD, 90. novocure, 91. Ockham oncology, 92. Premier-research, 93. Psi-cro, 94. Tetec-ag, 94. Tetec-ag, 95. Winicker-norimed, 96. Achaogen Inc, 97. ADIR, 98. AstraZenaca AB, 99. Demira Inc, 100. Euroscreen S.A., 101. Galmed Research and Development Ltd., 102. GETNE, 103. Guidant Europe NV, 104. Holaira Inc., 105. Immunomedics Inc., 106. Innate Pharma, 107. Isis Pharmaceuticals Inc, 108. Kantar Health GmbH, 109. MedImmune Inc, 110. Medpace Germany GmbH (CRO), 111. Merrimack Pharmaceuticals Inc, 112. Millenium Pharmaceuticals Inc, 113. Orion Corporation Orion Pharma, 114. Pharmacyclics Inc, 115. PIQUR Therapeutics Ltd, 116. Pulmonx International Sárl, 117. Servier (CRO), 118. SGS Life Science Services (CRO), 119. Treshold Pharmaceuticals Inc. There are no patents, products in development or marketed products to declare. This does not alter the authors' adherence to all the European Radiology policies on sharing data and materials.

Statistics and biometry No complex statistical methods were necessary for this paper.

Informed consent Written informed consent was obtained from all patients in this study.

Ethical approval Institutional Review Board approval was obtained.

Methodology
- prospective
- diagnostic or prognostic study (proof-of-concept study)
- performed at one institution

References

1. Rini BI, Campbell SC, Escudier B (2009) Renal cell carcinoma. Lancet 373:1119–1132
2. Kovacs G, Akhtar M, Beckwith BJ et al (1997) The Heidelberg classification of renal cell tumours. J Pathol 183:131–133
3. Ng CS, Wood CG, Silverman PM, Tannir NM, Tamboli P, Sandler CM (2008) Renal cell carcinoma: diagnosis, staging, and surveillance. AJR Am J Roentgenol 191:1220–1232
4. Delahunt B, McKenney JK, Lohse CM et al (2013) A novel grading system for clear cell renal cell carcinoma incorporating tumor necrosis. Am J Surg Pathol 37:311–322
5. Leveridge MJ, Finelli A, Kachura JR et al (2011) Outcomes of small renal mass needle core biopsy, nondiagnostic percutaneous biopsy, and the role of repeat biopsy. Eur Urol 60:578–584
6. Jayson M, Sanders H (1998) Increased incidence of serendipitously discovered renal cell carcinoma. Urology 51:203–205
7. Xi Y, Yuan Q, Zhang Y et al (2018) Statistical clustering of parametric maps from dynamic contrast enhanced MRI and an associated decision tree model for non-invasive tumour grading of T1b solid clear cell renal cell carcinoma. Eur Radiol 28:124–132
8. Nakamori S, Dohi K, Ishida M et al (2018) Native T1 mapping and extracellular volume mapping for the assessment of diffuse myocardial fibrosis in dilated cardiomyopathy. JACC Cardiovasc Imaging 11:48–59
9. Ulyte A, Katsaros VK, Liouta E et al (2016) Prognostic value of preoperative dynamic contrast-enhanced MRI perfusion parameters for high-grade glioma patients. Neuroradiology 58:1197–1208
10. Xu F, Chang K, Ma J et al (2017) The oncogenic role of COL23A1 in clear cell renal cell carcinoma. Sci Rep 7:9846
11. Lohi J, Leivo I, Oivula J, Lehto VP, Virtanen I (1998) Extracellular matrix in renal cell carcinomas. Histol Histopathol 13:785–796
12. Arheden H, Saeed M, Higgins CB et al (2000) Reperfused rat myocardium subjected to various durations of ischemia: estimation of the distribution volume of contrast material with echo-planar MR imaging. Radiology 215:520–528
13. Coy H, Young JR, Douek ML et al (2018) Association of qualitative and quantitative imaging features on multiphasic multidetector CT with tumor grade in clear cell renal cell carcinoma. Abdom Radiol (NY). https://doi.org/10.1007/s00261-018-1688-8
14. Ficarra V, Novara G, Galfano A et al (2009) The 'Stage, Size, Grade and Necrosis' score is more accurate than the University of California Los Angeles Integrated Staging System for predicting cancer-specific survival in patients with clear cell renal cell carcinoma. BJU Int 103:165–170

15. Campbell S, Uzzo RG, Allaf ME et al (2017) Renal mass and localized renal cancer: AUA Guideline. J Urol 198:520–529
16. Ljungberg B, Bensalah K, Canfield S et al (2015) EAU guidelines on renal cell carcinoma: 2014 update. Eur Urol 67:913–924
17. Karlo CA, Donati OF, Burger IA et al (2013) MR imaging of renal cortical tumours: qualitative and quantitative chemical shift imaging parameters. Eur Radiol 23:1738–1744
18. Yoshimitsu K, Honda H, Kuroiwa T et al (1999) MR detection of cytoplasmic fat in clear cell renal cell carcinoma utilizing chemical shift gradient-echo imaging. J Magn Reson Imaging 9:579–585
19. Baliyan V, Das CJ, Sharma R, Gupta AK (2016) Diffusion weighted imaging: technique and applications. World J Radiol 8:785–798
20. Bickel H, Pinker-Domenig K, Bogner W et al (2015) Quantitative apparent diffusion coefficient as a noninvasive imaging biomarker for the differentiation of invasive breast cancer and ductal carcinoma in situ. Invest Radiol 50:95–100
21. Rosenkrantz AB, Niver BE, Fitzgerald EF, Babb JS, Chandarana H, Melamed J (2010) Utility of the apparent diffusion coefficient for distinguishing clear cell renal cell carcinoma of low and high nuclear grade. AJR Am J Roentgenol 195:W344–W351
22. Lassel EA, Rao R, Schwenke C, Schoenberg SO, Michaely HJ (2014) Diffusion-weighted imaging of focal renal lesions: a meta-analysis. Eur Radiol 24:241–249
23. Hotker AM, Mazaheri Y, Wibmer A et al (2016) Use of DWI in the differentiation of renal cortical tumors. AJR Am J Roentgenol 206:100–105
24. Lopes Vendrami C, Parada Villavicencio C, DeJulio TJ et al (2017) Differentiation of solid renal tumors with multiparametric MR imaging. Radiographics 37:2026–2042
25. Kang SK, Zhang A, Pandharipande PV, Chandarana H, Braithwaite RS, Littenberg B (2015) DWI for renal mass characterization: systematic review and meta-analysis of diagnostic test performance. AJR Am J Roentgenol 205:317–324
26. Woo S, Suh CH, Kim SY, Cho JY, Kim SH (2017) Diagnostic performance of DWI for differentiating high- from low-grade clear cell renal cell carcinoma: a systematic review and meta-analysis. AJR Am J Roentgenol 209:W374–W381
27. Hu G, Liang W, Wu M et al (2018) Comparison of T1 mapping and T1rho values with conventional diffusion-weighted imaging to assess fibrosis in a rat model of unilateral ureteral obstruction. Acad Radiol. https://doi.org/10.1016/j.acra.2018.03.023
28. Friedli I, Crowe LA, Berchtold L et al (2016) New magnetic resonance imaging index for renal fibrosis assessment: a comparison between diffusion-weighted imaging and T1 mapping with histological validation. Sci Rep 6:30088
29. Robbers LF, Baars EN, Brouwer WP et al (2012) T1 mapping shows increased extracellular matrix size in the myocardium due to amyloid depositions. Circ Cardiovasc Imaging 5:423–426
30. Iles L, Pfluger H, Phrommintikul A et al (2008) Evaluation of diffuse myocardial fibrosis in heart failure with cardiac magnetic resonance contrast-enhanced T1 mapping. J Am Coll Cardiol 52:1574–1580
31. Klatt MG, Kowalewski DJ, Schuster H et al (2016) Carcinogenesis of renal cell carcinoma reflected in HLA ligands: a novel approach for synergistic peptide vaccination design. Oncoimmunology 5:e1204504
32. Ho TH, Serie DJ, Parasramka M et al (2017) Differential gene expression profiling of matched primary renal cell carcinoma and metastases reveals upregulation of extracellular matrix genes. Ann Oncol 28:604–610
33. Wan F, Wang H, Shen Y et al (2015) Upregulation of COL6A1 is predictive of poor prognosis in clear cell renal cell carcinoma patients. Oncotarget 6:27378–27387
34. Paudyal B, Paudyal P, Tsushima Y et al (2010) The role of the ADC value in the characterisation of renal carcinoma by diffusion-weighted MRI. Br J Radiol 83:336–343
35. White SK, Sado DM, Fontana M et al (2013) T1 mapping for myocardial extracellular volume measurement by CMR: bolus only versus primed infusion technique. JACC Cardiovasc Imaging 6:955–962